Structural and magnetic properties of large cobalt clusters

Jaime Souto-Casares,[1] Masahiro Sakurai,[1] and James R. Chelikowsky[1,2]
[1]*Center for Computational Materials, Institute for Computational Engineering and Sciences, University of Texas at Austin, Austin, Texas 78712, USA*
[2]*Departments of Physics and Chemical Engineering, University of Texas at Austin, Austin, Texas 78712, USA*
(Received 12 March 2016; published 20 May 2016)

We use a real-space implementation of pseudopotentials within the density functional theory to investigate the structural and magnetic properties of cobalt clusters with up to 365 atoms. We find from structural optimization that hcp and icosahedral clusters are lower in energy than bcc and fcc clusters. The calculated magnetic moments generally decrease as a function of increasing cluster size. For clusters of several hundred atoms the bulk limit becomes apparent. However, the decrease is not monotonic. It depends on the details of the interior structure of the cluster and the corresponding surface geometry. By analyzing the detailed evolution of the local magnetic moment, we find the spin moment is bulklike in the cluster interior and increases in the vicinity of the surface and can be correlated with coordination. The calculated behavior accounts for the observed variations in the measured moments.

DOI: 10.1103/PhysRevB.93.174418

I. INTRODUCTION

Magnetic ordering in low-dimensional systems has been the subject of study since the mid-1950s [1,2], where superparamagnetic behavior was first described and analyzed. With the subsequent development of synthesis techniques for nanomaterials in the latter half of the 20th century, it has become a field of intense research, particularly focused on magnetic transition metals such as cobalt, iron, and nickel, the most notable elemental ferromagnets [3–5]. A good understanding of the magnetism in nanostructured metal clusters is not only of great importance in basic physics, but also of practical importance for numerous applications in data storage, spin transport, or catalysis, to cite a few (see Ref. [6] and references within).

Microscopically, the magnetic moment of a nanocluster has two main contributions: the spin moment, a major contribution, which arises from imbalance between spin-up and spin-down electrons, and the orbital moment, a minor contribution, which originates from the spin-orbit interaction in the absence of an external magnetic field. In clusters, the presence of a large surface area offers the possibility of an enhancement of the spin moment. Thanks to a weaker orbital hybridization near the surface, the 3*d* states tend to remain localized, forming narrower bands than those in the bulk. Magnetic moments per atom for clusters of Fe, Co, and Ni less than a few hundred atoms are notably enhanced when compared with bulk [7].

It has also been well established both theoretically [4,8–16] and experimentally [7,17–28] that, when presented as a function of the cluster size, the magnetic moment shows a complex nonmonotonic decay from the relatively large atomlike value until converging to the bulk limit. The local maxima and minima of the moments occur at different sized clusters, i.e., clusters with "magic" numbers of atoms. Moreover, not only size but also crystal structure, surface geometry, and nucleation center appear to be crucial factors determining the magnetic behavior of a system as well.

Granted the numerous advances made through these decades, a complete explanation of the mechanism under the nonmonotonic behavior of the magnetic moment is still a work in progress. Calculations performed so far have been limited to selected small clusters owing to the intense computational load involved, and the predicted results often exhibit important discrepancies among themselves [8,10,11,14,29–35]. Moreover, despite its great relevance, available experimental techniques remain unable to give a complete description of these phenomena [15,25,36]. Specifically, experimental methods cannot provide us detailed structural information for a cluster of a given size nor confirm whether the cluster is in structural equilibrium.

Here, we investigate the stability of large Co clusters (with up to 365 atoms) in various structural motifs by performing first-principles electronic-structure calculations. Such clusters offer a notable challenge from a computational point of view. The size of the Hamiltonian matrix is effectively doubled with respect to a non-spin-polarized calculation. Moreover, the seven *d* electrons per Co atom create highly energetic states, which hinders structural relaxations. We compute magnetic moments and compare them to measurements, and analyze the evolution of local magnetic moments from the center of a cluster to its surface.

II. COMPUTATIONAL METHOD

We performed these calculations using PARSEC [37–39], a real-space implementation of pseudopotentials within the density functional theory [40,41]. PARSEC solves the Kohn-Sham equation for the electronic structure in a self-consistent manner directly in real space on an orthogonal, uniform, three-dimensional grid. One of the key aspects of PARSEC is the use of high-order finite-difference expansion for the kinetic operator of the Hamiltonian. This treatment is allowed by the real-space formalism and simplifies greatly the formulation of the problem and the convergence of the calculations when compared with other methods such as finite elements.

Computationally, the main task is to diagonalize the Hamiltonian matrix, which is a highly sparse matrix. The off-diagonal elements come from two contributions: the nonlocal part of the pseudopotential (localized area around each atom) and the high-order finite-difference expansion terms from

the Laplacian (typically 6th to 8th order is used). In earlier versions of PARSEC, we employed a direct diagonalization using public domain iterative eigensolvers like ARPACK [42] or TRLANC [43]. In the current vesion of PARSEC, we use an alternate algorithm crafted for our real-space problem. Specifically, we use a subspace filtering iteration based on expanding the Hamiltonian matrix with Chebyshev polynomials [44,45]. This algorithm can improve the timing by 1 order of magnitude with respect to previous methods [44,45]. To initiate the process, we need only an approximate eigenvalue spectrum to construct the subspace polynomials [44,45].

Real-space methods possess a number of important features compared to a plane-wave formalism, which has been traditionally the most widely used approach [46]. First, the semilocality of real-space methods allows for a simple and yet powerful parallelization scheme: the partition of the simulation cell and the assignment of each processor to work on a single subdivision. This parallelization is well optimized, since communications among processors occur in the boundaries of each sector. Second, periodic boundary conditions, which are a natural consequence of the use of a basis such as plane waves, are no longer needed. When an isolated system is considered, confined boundary conditions are a natural choice. The wave functions are required to vanish beyond a certain distance from the system, forming a sphere with radius 10 a.u. removed from the outermost atom. We also require the Hartree potential to match a multipole expansion of the electrostatic potential at the domain boundary. The absence of a supercell geometry, as used in plane-wave methods, removes any interactions among periodic replicas. As such, the size of the domain can be notably reduced and, although we do not consider charged clusters in this work, long-range Coulomb potentials are easily handled in real-space methods [38].

We take the exchange-correlation potential from the generalized gradient approximation (GGA) as parametrized by Perdew, Burke, and Ernzerhof [47,48]. This approximation works well for moderately correlated systems such as iron [16]. We express the electron-ion interaction using norm-conserving pseudopotentials cast in the form of Troullier-Martins, [49] with a reference configuration $[\mathrm{Ar}]4s^2 3d^7 4p^0$ for cobalt. The core radii are given by $r_s = 2.18$ a.u., $r_d = 2.18$ a.u., and $r_p = 2.38$ a.u. (1 a.u. $= 0.529\,2$ Å). For the real-space grid, only one parameter is needed to control convergence: the spacing between adjacent points of the grid. In the present work we use a grid spacing of 0.29 a.u. For the purposes of comparison to bulk phases, we can also do real-space computations for periodic systems, just as in the case of plane waves. In that case, we alter the boundary conditions.

III. RESULTS

A. Geometry

Bulk cobalt crystallizes in a hcp structure under ambient conditions [50,51]. Above 700 K, Co undergoes a phase transition to a fcc structure, also ferromagnetic [51,52], whereas under pressure (105 GPa) this phase is believed to suppress its magnetic properties [52]. Further studies investigating the phase diagram of bulk Co confirm its structural complexity [53] and motivates the investigation of clusters with a wide set of geometries.

Co in bcc phase has been grown in the form of thin films on GaAs substrate [54–58]. It is believed that its finite nature and surface effects are responsible for the the successful stabilization of a 357-Å-thick film [56]. bcc-Co has also been found to form naturally as a precipitation in supersaturated $Au_{90}Co_{10}$ [59]. Theoretical calculations on bcc-Co have been scarce [13,60,61], focusing typically on the metastability of this phase [62]. In clusters, the photoionization experiment with mass spectrometry analysis supports the existence of icosahedral Co clusters [26] up to 800 atoms.

Here, we consider four kinds of motifs for atomic clusters: icosahedral, hcp, fcc, and bcc. Although growth of an icosahedral cluster involves an fcc packing in attaching atoms on surfaces, the cluster does not possess fcc symmetry as a whole, and adjacent triangular faces meet at a slightly distorted angle. Complete filling of the nth atomic shell of an icosahedral cluster needs $10n^2 + 2$ atoms, yielding a perfect cluster of N atoms where $N = (10n^3 + 15n^2 + 11n + 3)/3 = 13,55,147,309,\ldots$. By construction, one atom is located at the center of an icosahedral cluster. Clusters with hcp and fcc structures are chosen to be centered on an atomic site. The shape of some faceted fcc clusters is a polyhedron with eight triangular faces and six square faces, i.e., a cuboctahedron, which can be regarded as an isomer of icosahedron. We explore three types of bcc clusters with different centers: an atom-centered bcc cluster; a bond-centered bcc cluster that has a nucleation point at the middle of two neighboring atoms; and an interstitial-centered bcc cluster whose center coincides with the face center of the bcc unit cell.

For each center, cubic clusters are created by filling the first closed shells (9, 35, 91, 189, 341 for atom-centered; 30, 84, 180, 330 for interstitial-centered; and 28, 92, 206, 298 for bond-centered). Several clusters are created out of the aforementioned sets just by removing those atoms located outside of imaginary spheres of decreasing radius. With this method, we create a total number of 61 bcc clusters with different surface geometries, ranging from perfect cubes to spheres.

We perform structural optimizations for all clusters using the Broyden-Fletcher-Goldfarb-Shanno algorithm [63–65]. Since atoms near the surface feel larger forces than inner atoms before structural relaxation, they undergo a large amount of atomic displacement during minimization of total energy and forces. After optimization, the residual forces are typically less than 0.01 Ry/a.u.

B. Energetics

In Fig. 1, total energies of geometry-optimized cobalt clusters are plotted as a function of cluster size. The energy reference is the bulk energy of hcp Co, and the value is calculated using the PARSEC code with the same Co pseudopotential, a grid spacing of 0.16 a.u., and a $7 \times 7 \times 4$ k-point mesh. The solid curve in Fig. 1 is fitted to the values of four perfect icosahedral clusters using polynomials, and it goes to zero at around a cluster size of 1500.

With increasing cluster size, the total energy decreases overall. However, oscillations associated with the cluster

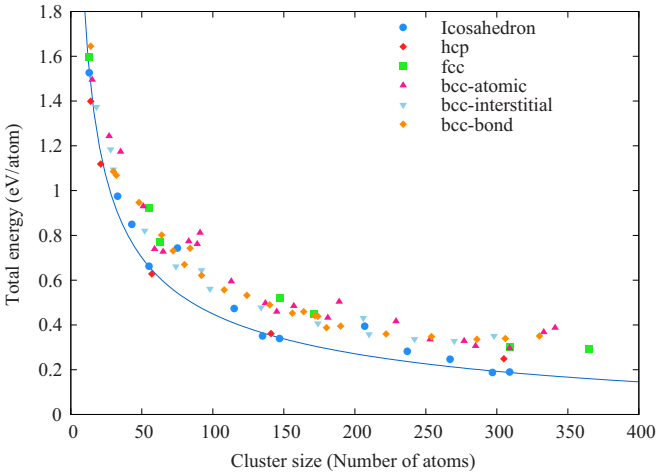

FIG. 1. Total energies of geometry-optimized cobalt clusters with six different structures are plotted as a function of cluster size. Energy is measured from that of bulk hcp phase. The curve is fitted to the values of perfect icosahedral clusters (see text).

shape and surface morphology occur. Among the clusters we examined (up to 365 atoms), small faceted icosahedral clusters and hcp clusters are found to be lower in energy than the others, indicating that they are candidates for stable structures in this size range. They have a small surface-to-volume ratio and their shapes are nearly spherical. The total energy of icosahedral clusters oscillates with a period corresponding to a complete filling of an atomic shell. Local minima in energy lie at around 55, 147, and 309 atoms, where the cluster is a perfect (closed-shell) icosahedron. The total energies of three families of bcc clusters show similar size dependence each other, implying that the innermost structure around the cluster center plays a minor role in determining its energy. For the atom-centered bcc clusters, perfect cubic ones give the local energy maxima located at sizes of 91, 189, and 341. The fcc clusters are systematically higher in energy than icosahedral and hcp clusters. Except for the smallest 13-atom cluster, as the cluster size gets larger, the energy difference between icosahedral and cuboctahedral isomers becomes smaller.

C. Total magnetic moments

We examine the interplay of structural relaxation with the magnetic moment of a cluster. On relaxing the structure, accompanied by a movement of protruding atoms on the cluster surface, the $3d$ bands get a more dispersive character, resulting in reduction of the net magnetic moment. After relaxation, the change in the bond length is a few percent within the initial value, and the change in the magnetic moment ranges from an $\sim$5% decrease to an $\sim$1% increase compared to the initial value.

We only take into account the spin moment of the cluster and do not include orbital contribution, whereas the experimental value is a total moment, a summation of the spin and orbital moment. In bulk Co, orbital effects cause a shift in the gyromagnetic ratio (so-called g factor), yielding an effective gyromagnetic ratio $g = 2.25$ ($g = 2.0$ for a free electron). We assume Co clusters possess a similar degree of orbital

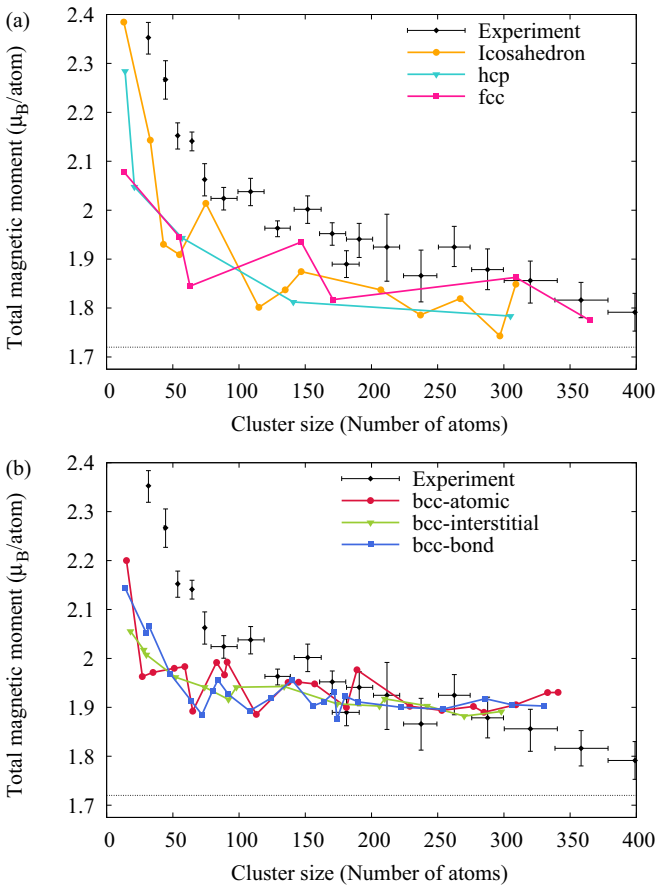

FIG. 2. Calculated magnetic moments per atom compared to the experimental data taken from Ref. [17]. The dotted line indicates the value of the magnetic moment per atom in bulk cobalt (1.72 μ_B/atom).

contributions, i.e., the orbital moment of the cluster should contribute less than 10% of the spin moment.

Figure 2(a) shows magnetic moments per atom in units of Bohr magneton μ_B as a function of size for the icosahedral, hcp, and fcc clusters. For comparison, we also plot the experimental data by Billas and co-workers [17]. Although the magnetic moments are systematically underestimated due to lack of the orbital moment, the overall size dependencies of the moments obtained for three cluster families are consistent with the experiment. In particular, the behavior of the moment at around sizes 130 and 240 are well described in the icosahedral family. We find no correlation between the local minimum (maximum) of the moment and the number of facets. The calculated moments for fcc clusters are in good agreement with the size dependence at around 150 as well as the converged behavior for more than 300 atoms. In the fcc family, cuboctahedral clusters are found to have a larger moment than icosahedral isomers. The moments obtained for the hcp clusters are within the range of those for the icosahedral and fcc clusters.

In Fig. 2(b), the bcc clusters with three different centers exhibit similar size dependence, indicating that the nucleation center also plays a minor role in determining the magnetic moment of a cluster. Regardless of the center structure, small

bcc clusters are predicted to have an enhanced magnetic moment, being qualitatively consistent with the experiment. For clusters larger than 200 atoms, however, the calculated moments are practically constant, resulting in an overestimate of the moment. In the atom-centered family, local maxima of the moment observed at sizes 91, 189, and 341 are associated with perfect cubic clusters.

D. Local magnetic moment

The local magnetic moment of a particular atom j is computed as the integral of the spin density within a spherical domain surrounding it, Ω_j:

$$\mu_j^{\text{local}} = \int_{\Omega_j} [\rho_\uparrow(\vec{r}) - \rho_\downarrow(\vec{r})] d^3\vec{r} \quad .$$

Here, $\rho_\uparrow/\rho_\downarrow$ represents the electronic density for the majority (minority) spin. Since the main source of this spin imbalance resides with the $3d$ orbitals, the local magnetic moment tends to be very localized. This is confirmed by our calculations, where the sum of the local magnetic moments lies always within a 10% range from total magnetic moment. Therefore, the radius for the integration sphere is set to be half the minimum bond length found in the cluster.

It is well known that the local magnetic moment of a particular atom is related to its coordination within the structure, increasing its value when decreasing the number of neighbors. The isolated atom can be regarded as a limiting case with maximum local magnetic moment, given by Hund's rule. When interaction with other atoms leads to a delocalized state, the corresponding magnetic moment decays until it reaches its bulk coordination number. However, the magnetic properties are very sensitive to the structural properties, such as local coordination and facet geometry, and a detailed description of their relation is still lacking. For example, Jensen and Benneman [66] attempted an explanation of the oscillations of the magnetic moment with the cluster size using the magnetic shell model framework [7]. They assumed the atomic magnetic moments depend only on the atomic environment, with a monotonic relation with the coordination number. This simple model captures some of the features drawn by the experimental results, but some discrepancies with their approach are quite notable.

Figure 3 shows the averaged value of the local magnetic moment of the atoms for a selected set of example clusters as a function of their coordination number. Dashed lines indicate the range of the minimum and maximum magnetic moments. The solid lines displayed on the plots correspond to linear fits of the calculations. Our calculations do not support a hypothesis of a simple linear relationship between coordination number and local magnetic moment, but they do show a strong correlation of the two. For instance, the individual correlation values for the bcc and icosahedral structures remain >0.9 (with several exceptions between the range $0.8 < r < 0.9$: the 27 atom for the bcc atomic; 28 and 30 atom for the bcc bond; 43, 75, and 237 atom for the icosahedral). The averaged slope for the bcc and icosahedral families is $-0.034\,6 \pm 0.086\,\mu_B$. Despite the difference in ranges of the coordination number, the lines corresponding to the bcc family [panels (a) and (b) in Fig. 3] lie close to the one calculated for the icosahedrons [panel (c)]. However, this behavior gets more convoluted for the other two structures considered in this paper, as one can see in Fig. 3(d) for the 305-atom hcp cluster as a representative example.

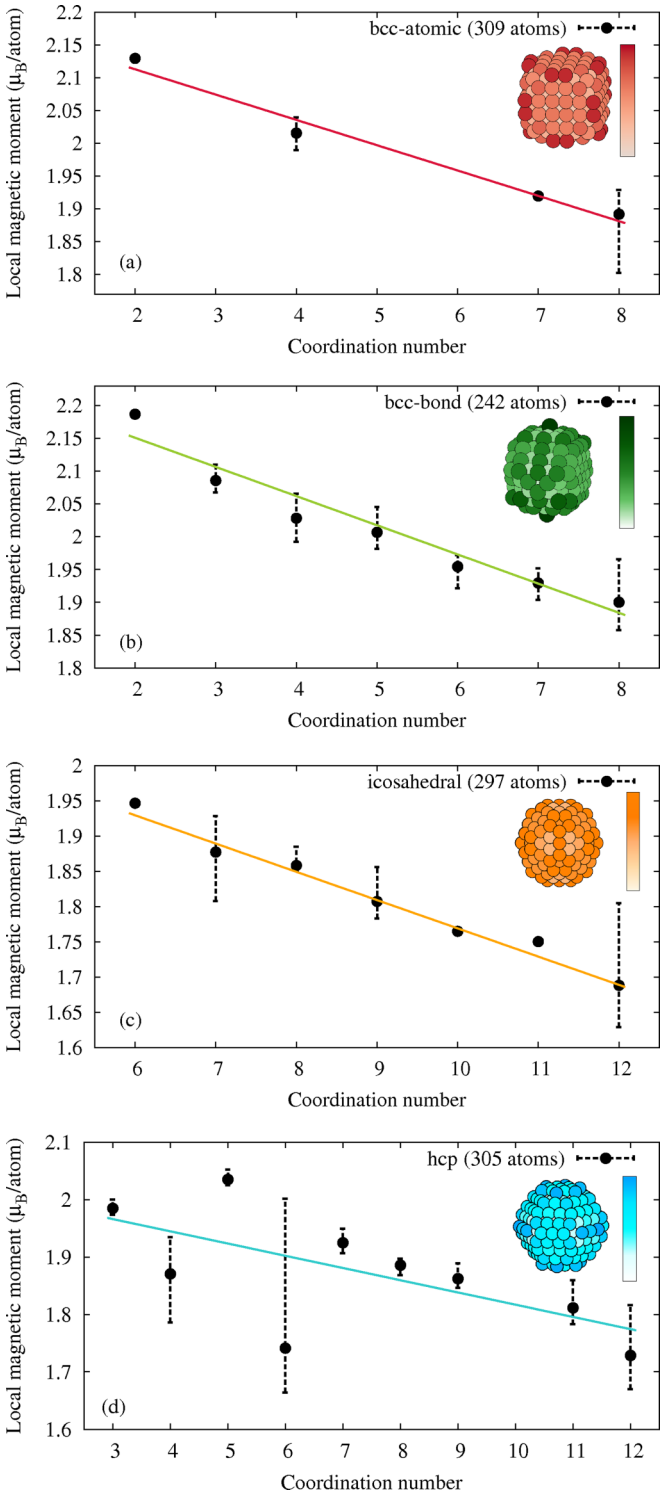

FIG. 3. Local magnetic moment per atom with respect to the coordination number. Error bars represent the minimum and maximum value. Each set of points has been fitted to a line. A miniature of the specific cluster is shown, with the color map representing the individual local magnetic moment growing in the upper direction.

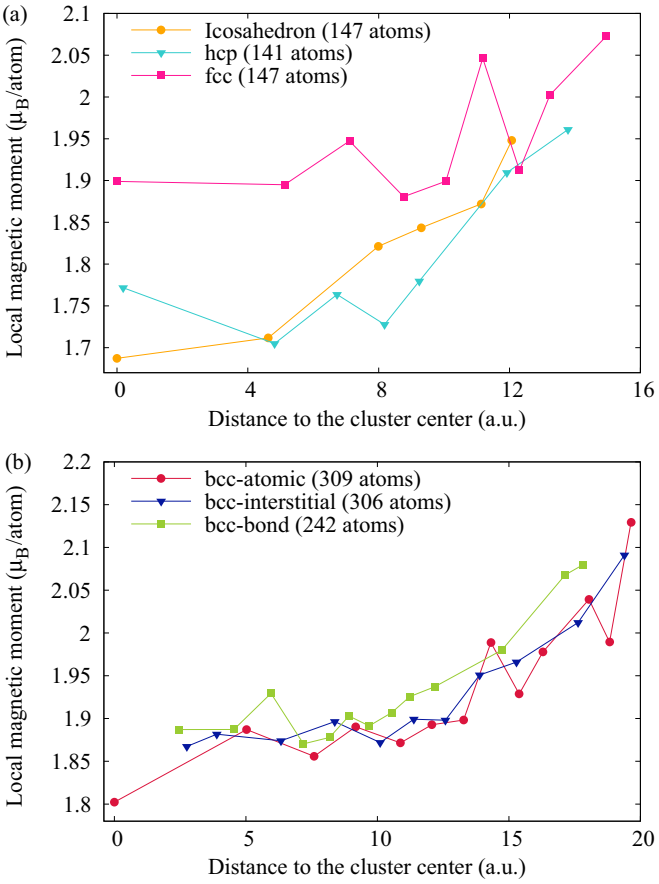

FIG. 4. Evolution of local magnetic moment per atom from center to surface for a set of example cluster from the six structures considered in this work.

Figure 4 shows the evolution of the local magnetic moment as a function of the distance to the center of the cluster. As expected, the trend exhibits a general increase when going from the center towards the surface. One can differentiate two regions: (i) a plateau corresponding to those points located in the inner shells of the cluster, with bulk coordination number; (ii) a regime for those atoms near the surface of the cluster. Such atoms have a reduced coordination number and show an increase of their magnetic moment. The three bcc clusters shown in Fig. 4(b) have a similar number of atoms and their curves are almost superimposed. The boundary between the two regions can be traced roughly to around ∼14 a.u., precisely the distance to the first atom with a coordination less than the value for bulk. The same situation occurs for those clusters in Fig. 4(a), each one for a different distance (∼8 a.u. for icosahedron, ∼5 a.u. for hcp, and ∼11 a.u. for fcc). It is also worth noting the lower value that the icosahedral and hcp curves have in the bulk region (around $1.7\,\mu_B$) owing to the higher coordination of these structures with respect to the fcc and bcc curves (around $1.9\,\mu_B$). The oscillatory behavior shown on the growing part of the curves can be easily accounted for considering that atoms with a lower coordination may be further away from the center than others with higher coordination.

IV. SUMMARY AND CONCLUSIONS

We have investigated the structural and magnetic properties of cobalt clusters of up to 365 atoms using a real-space formalism of pseudopotentials within the density functional theory. The hcp and icosahedral clusters, which are spherical with small surface-to-volume ratios, are found to be the most stable. The calculated magnetic moments for hcp and icosahedral clusters reproduce not only the overall decreasing trend but also exhibit some fine size dependencies, which are observed in experiment. We also analyzed the distribution of the local magnetic moment on the cluster. When compared as a function of the distance to the center of the structure, we find two distinct regimes, one "bulklike" inside, almost constant, and another describing the surface atoms where the magnetic moment experiences a strong enhancement. The main features of this relation can be explained by the dependency of the local magnetic moment of an atom with its coordination number.

ACKNOWLEDGMENTS

Our work is supported by the National Science Foundation, DMR 1435219. Computational resources have been provided by the Texas Advanced Computing Center (TACC) and the National Energy Research Scientific Computing Center (NERSC).

[1] C. P. Bean, J. Appl. Phys. **26**, 1381 (1955).
[2] C. P. Bean and J. D. Livingston, J. Appl. Phys. **30**, S120 (1959).
[3] X. Batlle and A. Labarta, J. Phys. D: Appl. Phys. **35**, R15 (2002).
[4] J. A. Alonso, Chem. Rev. (Washington, DC, U. S.) **100**, 637 (2000).
[5] R. H. Kodama, J. Magn. Magn. Mater. **200**, 359 (1999).
[6] J. I. Martín, J. Nogués, K. Liu, J. L. Vicent, and I. K. Schuller, J. Magn. Magn. Mater. **256**, 449 (2003).
[7] I. M. L. Billas, A. Châtelain, and W. A. de Heer, Science **265**, 1682 (1994).
[8] F. Aguilera-Granja, A. Vega, and L. C. Balbás, Chem. Phys. **415**, 106 (2013).
[9] A. N. Andriotis and M. Menon, Phys. Rev. B **57**, 10069 (1998).
[10] S. Datta, M. Kabir, S. Ganguly, B. Sanyal, T. Saha-Dasgupta, and A. Mookerjee, Phys. Rev. B **76**, 014429 (2007).
[11] C. D. Dong and X. G. Gong, Phys. Rev. B **78**, 020409 (2008).
[12] N. Fujima and S. Sakurai, J. Phys. Soc. Jpn. **68**, 586 (1999).
[13] J. Guevara, F. Parisi, A. M. Llois, and M. Weissmann, Phys. Rev. B **55**, 13283 (1997).
[14] R. Singh and P. Kroll, Phys. Rev. B **78**, 245404 (2008).
[15] J. L. Rodríguez-López, F. Aguilera-Granja, K. Michaelian, and A. Vega, Phys. Rev. B **67**, 174413 (2003).
[16] M. L. Tiago, Y. Zhou, M. M. G. Alemany, Y. Saad, and J. R. Chelikowsky, Phys. Rev. Lett. **97**, 147201 (2006).
[17] I. M. L. Billas, A. Châtelain, and W. A. de Heer, J. Magn. Magn. Mater. **168**, 64 (1997).

[18] J. P. Bucher, D. C. Douglass, and L. A. Bloomfield, Phys. Rev. Lett. **66**, 3052 (1991).
[19] D. C. Douglass, A. J. Cox, J. P. Bucher, and L. A. Bloomfield, Phys. Rev. B **47**, 12874 (1993).
[20] P. Gambardella, S. Rusponi, M. Veronese, S. S. Dhesi, C. Grazioli, A. Dallmeyer, I. Cabria, R. Zeller, P. H. Dederichs, K. Kern, C. Carbone, and H. Brune, Science **300**, 1130 (2003).
[21] M. B. Knickelbein, J. Chem. Phys. **125**, 044308 (2006).
[22] A. Langenberg, K. Hirsch, A. Ławicki, B. Zamudio-Bayer, M. Niemeyer, P. Chmiela, B. Langbehn, A. Terasaki, B. v. Issendorff, and J. T. Lau, Phys. Rev. B **90**, 184420 (2014).
[23] J. Meyer, M. Tombers, C. v. Wüllen, G. Niedner-Schatteburg, S. Peredkov, W. Eberhardt, M. Neeb, S. Palutke, M. Martins, and W. Wurth, J. Chem. Phys. **143**, 104302 (2015).
[24] R. Morel, A. Brenac, C. Portemont, T. Deutsch, and L. Notin, J. Magn. Magn. Mater. **308**, 296 (2007).
[25] F. W. Payne, W. Jiang, J. W. Emmert, J. Deng, and L. A. Bloomfield, Phys. Rev. B **75**, 094431 (2007).
[26] M. Pellarin, B. Baguenard, J. L. Vialle, J. Lermé, M. Broyer, M. Miller, and A. Perez, Chem. Phys. Lett. **217**, 349 (1994).
[27] X. Xu, S. Yin, R. Moro, and W. A. de Heer, Phys. Rev. Lett. **95**, 237209 (2005).
[28] X. Xu, S. Yin, R. Moro, A. Liang, J. Bowlan, and W. A. de Heer, Phys. Rev. Lett. **107**, 057203 (2011).
[29] A. H. Pakiari and R. Dehghanpisheh, Struct. Chem. **27**, 583 (2016).
[30] I. Hamid, M. Fang, and H. Duan, AIP Adv. **5**, 047129 (2015).
[31] L. Liu, Y. Su, J. Gao, and J. Zhao, Phys. E (Amsterdam, Neth.) **46**, 6 (2012).
[32] S. D. Borisova, G. G. Rusina, and E. V. Chulkov, Phys. Solid State **52**, 838 (2010).
[33] S. Sahoo, A. Hucht, M. E. Gruner, G. Rollmann, P. Entel, A. Postnikov, J. Ferrer, L. Fernandez-Seivane, M. Richter, D. Fritsch, and S. Sil, Phys. Rev. B **82**, 054418 (2010).
[34] A. Sebetci, Chem. Phys. **354**, 196 (2008).
[35] Q.-M. Ma, Z. Xie, J. Wang, Y. Liu, and Y.-C. Li, Phys. Lett. A **358**, 289 (2006).
[36] X. Yie and J. A. Blackman, J. Phys.: Condens. Matter **16**, 4373 (2004).
[37] J. R. Chelikowsky, J. Phys. D: Appl. Phys. **33**, R33 (2000).
[38] L. Kronik, A. Makmal, M. L. Tiago, M. M. G. Alemany, M. Jain, X. Huang, Y. Saad, and J. R. Chelikowsky, Phys. Status Solidi B **243**, 1063 (2006).
[39] A. Natan, A. Benjamini, D. Naveh, L. Kronik, M. L. Tiago, S. P. Beckman, and J. R. Chelikowsky, Phys. Rev. B **78**, 075109 (2008).
[40] P. Hohenberg and W. Kohn, Phys. Rev. **136**, B864 (1964).
[41] W. Kohn and L. Sham, Phys. Rev. **140**, A1133 (1965).
[42] R. B. Lehoucq, K. Maschhoff, D. Sorensen, and C. Yang, the ARPACK software package, http://www.caam.rice.edu/software/ARPACK/.
[43] K. Wu, A. Canning, H. D. Simon, and L.-W. Wang, J. Comput. Phys. **154**, 156 (1999).
[44] Y. Zhou, Y. Saad, M. L. Tiago, and J. R. Chelikowsky, Phys. Rev. E **74**, 066704 (2006).
[45] Y. Zhou, Y. Saad, M. L. Tiago, and J. R. Chelikowsky, J. Comput. Phys. **219**, 172 (2006).
[46] M. C. Payne, M. P. Teter, D. C. Allan, T. A. Arias, and J. D. Joannopoulos, Rev. Mod. Phys. **64**, 1045 (1992).
[47] J. P. Perdew, K. Burke, and M. Ernzerhof, Phys. Rev. Lett. **77**, 3865 (1996).
[48] J. P. Perdew, K. Burke, and M. Ernzerhof, Phys. Rev. Lett. **80**, 891 (1998).
[49] N. Troullier and J. L. Martins, Phys. Rev. B **43**, 1993 (1991).
[50] D. A. Young, *Phase Diagrams of the Elements* (University of California Press, Livermore, CA, 1991).
[51] C. S. Yoo, P. Söderlind, and H. Cynn, J. Phys.: Condens. Matter **10**, L311 (1998).
[52] C. S. Yoo, H. Cynn, P. Söderlind, and V. Iota, Phys. Rev. Lett. **84**, 4132 (2000).
[53] M. M. Armentrout and A. Kavner, J. Appl. Phys. **118**, 194904 (2015).
[54] G. A. Prinz, Phys. Rev. Lett. **54**, 1051 (1985).
[55] Y. U. Idzerda, D. M. Lind, D. A. Papaconstantopoulos, G. A. Prinz, and B. T. Jonker, J. Appl. Phys. **64**, 5921 (1988).
[56] Y. U. Idzerda, W. T. Elam, B. T. Jonker, and G. A. Prinz, Phys. Rev. Lett. **62**, 2480 (1989).
[57] N. Spiridis, T. Ślęzak, M. Zajac, and J. Korecki, Surf. Sci. **566-568**, 272 (2004).
[58] M. Ohtake, O. Tabuhara, and J. Higuchi, J. Appl. Phys. **109**, 07C105 (2011).
[59] R. Bauer, E. Bischoff, and E. J. Mittemeijer, Phys. Rev. B **81**, 094113 (2010).
[60] B. I. Min, T. Oguchi, and A. J. Freeman, Phys. Rev. B **33**, 7852 (1986).
[61] D. J. Singh, Phys. Rev. B **45**, 2258 (1992).
[62] A. Y. Liu and D. J. Singh, J. Appl. Phys. **73**, 6189 (1993).
[63] R. H. Byrd, P. Lu, and J. Nocedal, SIAM J. Sci. Comput. **16**, 1190 (1995).
[64] C. Zhu, R. H. Byrd, and J. Nocedal, ACM Trans. Math. Software **23**, 550 (1997).
[65] J. L. Morales and J. Nocedal, ACM Trans. Math. Software **38**, 1 (2011).
[66] P. Jensen and K. H. Benneman, Z. Phys. D: At., Mol. Clusters **35**, 273 (1995).